

Automated third generation squark production to next-to-leading order

Dorival Gonçalves,¹ David López-Val,² Kentarou Mawatari,³ and Tilman Plehn⁴

¹*Institute for Particle Physics Phenomenology, Department of Physics, Durham University, United Kingdom*

²*Centre for Cosmology, Particle Physics & Phenomenology CP3, Université catholique de Louvain, Belgium*

³*Theoretische Natuurkunde and IIHE/ELEM, Vrije Universiteit Brussel, Belgium
and International Solvay Institutes, Brussels, Belgium*

⁴*Institut für Theoretische Physik, Universität Heidelberg, Germany*

(Dated: September 22, 2018)

If light-flavor squarks and gluinos are indeed heavy and chargino pair production is plagued with overwhelming backgrounds, pair production and associated production of stops and charginos will become the key signatures in the upcoming LHC runs. We present fully automated next-to-leading order predictions for heavy flavor squark production at the LHC, including stop–chargino associated production, based on MADGOLEM. We compute the total and differential NLO rates for a variety of MSSM scenarios with a light third generation. We focus on theoretical uncertainties on differential rates, including a comparison to multi-jet merging and the impact of bottom parton densities for stop–chargino associated production. We find that for the associated production channel the rates can reach tens of femtobarns, but the scale dependence does not provide a conservative estimate of the theoretical uncertainties.

Contents

I. Introduction	2
II. Setup	3
III. Results	4
A. Stop and sbottom pair production	4
B. Associated stop–chargino production	6
C. 4-flavor versus 5-flavor schemes	8
IV. Summary	9
A. Renormalization	10
References	15

I. INTRODUCTION

After the discovery of a light, likely fundamental Higgs scalar, supersymmetry (SUSY) as a solution to the hierarchy problem is still among the most cherished paradigms for physics beyond the Standard Model (SM) [1]. In relation to experimental results supersymmetry provides dark matter candidates and a pathway towards gauge coupling unification. Notwithstanding, TeV-scale SUSY is in growing tension with the Run-I LHC results [2]. Inclusive searches are largely governed by light-flavor squarks and gluino production and provide exclusion limits for example of the kind $m_{\tilde{q}} \simeq m_{\tilde{g}} \simeq 1.5$ TeV or $m_{\tilde{g}} \simeq 1.2$ TeV for $m_{\tilde{g}} \ll m_{\tilde{q}}$ in the squark-gluino mass plane [3–5]. In comparison, the limits on direct stop pair production as well as direct neutralino and chargino production hardly affect the supersymmetric parameter space. Be as it may, the inclusive search strategies do not cover the whole MSSM parameter space and motivate more flexible approaches for the upcoming LHC runs.

In particular third-generation squarks with their direct link to the hierarchy problem are being searched for in dedicated analyses. Renormalization group effects as well as squark mixing tend to make one top squark especially light [6–10]. To avoid the gauge link between left-handed stops and sbottoms such a light stop will typically be right-handed. In dark matter models a light top squark can co-annihilate with a bino-like neutralino, giving the correct relic density for a $\mathcal{O}(10)$ GeV mass splitting [11]. In the context of electroweak baryogenesis, light stops may allow for the required first-order phase transition and pull down the critical temperature to protect the baryon asymmetry from washout [12]. All of this points to scenarios, where at least one third generation squark and the electroweak gauginos and Higgsinos are relatively light, while light-flavor squarks and gluinos are too heavy to be observed at the LHC during an early 14 TeV run.

The LHC results from the 7 TeV and 8 TeV runs translate into exclusion limits in the $\tilde{t}_1 - \tilde{\chi}_1^0$ mass plane. Assuming R-parity conservation with the lightest stop as the next-to-lightest supersymmetric partner (NLSP) the decay mode $\tilde{t}_1 \rightarrow t\tilde{\chi}_1^0$ requires $m_{\tilde{t}_1} \gtrsim 600$ GeV. This limit weakens to $m_{\tilde{t}_1} \gtrsim 450$ GeV for heavy neutralinos, similarly to the case when the decay mode $\tilde{t}_1 \rightarrow b\tilde{\chi}_1^\pm$ opens [13–15]. Compressed spectra reduce the experimental reach even further, leading to allowed top masses just above the top mass [16]. The latter can then be searched for in leptonic decay channels [17], hadronic decay channels [18], or new associated production channels [19]. Obviously, pair production of the light(est) third generation squark should come with a large LHC cross section. On the other hand, we will see that associated stop-chargino production can give rise to sizeable event numbers and can therefore play a key role in searches for neutralinos and charginos. Moreover, through their off-shell effects the three production processes, namely stop pair production, chargino pair production, and associated stop-chargino production are closely tied at the next-to-leading order (NLO) level.

The challenge in LHC analyses assuming very specific supersymmetric particle spectra is the availability of precision predictions. For example, the original theoretical studies of squark production at hadron colliders usually assume degenerate squark masses [20–24]. The NLO computation of stop pair production allows for separate stop masses [25]. More recently, improved predictions have become available including electroweak [26], higher-order QCD [27] and resummed corrections [28] mostly assuming simplified supersymmetric mass patterns. Efforts in matching fixed-order NLO predictions to parton showers are presently underway [29]. In this paper we discuss the extension of automatized MADGOLEM setup [30–32] to third generation squark rates, including bottom densities, to NLO accuracy¹. The key advantage of this approach is its complete flexibility in the model assumptions which are defined in the MADGRAPH framework. Correspondingly, in this paper we for the first time provide precision predictions for fully exclusive event rates and with completely flexible model parameters for the upcoming LHC runs. Assuming for example a simplified model of top squarks and charginos/neutralinos the processes discussed in this paper together with chargino pair production will allow for a complete NLO treatment of LHC rates and distributions with MADGOLEM.

The remainder of this paper is organized as follows: in Section II we present the framework of our calculation, describing both the automated MADGOLEM setup and the MSSM benchmarks we use for our phenomenological analysis. In Section III the total and differential NLO rates are portrayed and analyzed for three representative processes: i) stop pairs $pp \rightarrow \tilde{t}_1\tilde{t}_1^*$; ii) sbottom pairs $pp \rightarrow \tilde{b}_1\tilde{b}_1^*$; and iii) associated stop-chargino production $pp \rightarrow \tilde{t}_1\tilde{\chi}_1^\pm$. The role of the incoming bottoms and their description within the 4-flavor and 5-flavor schemes is addressed in a dedicated subsection. We summarize our results in Section IV. Details on the renormalization scheme and analytical expressions for the relevant ultraviolet (UV) counterterms and renormalization constants are given in the Appendix.

¹ The MADGOLEM code with pre-compiled processes is available from the authors upon request.

II. SETUP

We compute the total and differential NLO rates, including all QCD and SUSY-QCD corrections in the fully automated MADGOLEM setup [30–32]. MADGOLEM is an independent, modular add-on to MADGRAPH [33, 34]. It generates all tree-level diagrams in the MADGRAPH v4.5 framework and uses QGRAF [35] and GOLEM [36, 37] for the one-loop amplitudes. The relevant counterterms, Catani–Seymour dipoles [38] and subtraction terms for on-shell divergences [23, 39] are part of the automated setup.

The NLO effects split into real and virtual corrections. Real corrections originate from radiation off the initial or final state. Their infrared (IR) divergences are subtracted by means of massive Catani–Seymour dipoles [38]. In addition to the SM dipoles MADGOLEM provides squark dipoles for final-final and final-initial singularities as an extension to MADDIPOLE [40]. We retain the dependence on the FKS-like cutoff α [41] to include more ($\alpha \rightarrow 1$) or less ($\alpha \ll 1$) of the finite phase space in the dipole subtraction. Our default choice is $\alpha = 1$.

Virtual corrections arise from gluons and gluinos. The standard 't Hooft–Feynman gauge for internal gluons avoids higher rank loop integrals. Dimensional regularization breaks supersymmetry via the mismatch between the two fermionic gluino components and the $(2 - 2\epsilon)$ degrees of freedom of the transverse gluon field. MADGOLEM restores it using finite counter terms [23, 42]. The renormalization of the third generation squark sector is more complex than for the first and second generations, due to massive quarks and the corresponding squark mixing. Details on the renormalization procedure are specified in the Appendix.

Finally, we need to remove divergences due to intermediate resonant states. One example is the well known appearance of on-shell gluinos as part of the NLO squark pair production via the three-body subprocess $qg \rightarrow \tilde{q}\tilde{g} \rightarrow \tilde{q}\tilde{q}^*q$ [23, 39]. The caveat is twofold: on the one hand, these configurations lead to a phase space divergence. On the other hand, they can give rise to double counting once all squark and gluino NLO production rates are combined. Following the PROSPINO scheme we remove the on-shell divergences locally through a point-by-point subtraction over phase space. Off-shell contributions in the zero-width limit are genuine parts of the NLO real emission. This procedure preserves the gauge invariance as well as the spin correlations between the intermediate particles and the final state. The subtraction terms in the corresponding MADOS module have a Breit–Wigner shape and are generated automatically. For further details we refer the reader to Appendix B of Ref. [31].

Throughout our calculation we use consistent LO and NLO parton densities given by CTEQ6L1 and CTEQ6M with five active flavors [43] for a 14 TeV LHC. For a dedicated analysis of the 4-flavor scheme in Section III C we resort to the NNPDF21_FFNNF4_100 [44] parton densities. The strong coupling constant $\alpha_s(\mu_R)$ is evaluated using 2-loop running from Λ_{QCD} to the required renormalization scale μ_R , again with five active flavors. Unless stated otherwise, we use a common central value of the average final state mass for the renormalization and factorization scales, $\mu_R = \mu_F \equiv \mu^0 = (m_1 + m_2)/2$. From previous studies we know this choice to yield perturbatively stable results [23].

So-called phenomenological MSSM (pMSSM) scenarios [45, 46] describe the supersymmetric parameter space featuring: i) R-parity and CP-conservation; ii) minimal flavor violation at the electroweak scale; iii) degenerate light-flavor squarks; and iv) negligible Yukawa couplings and trilinear interactions for the first and second generations. These requirements shrink the general MSSM parameter space to 19 free parameters, while they do not demand any specific assumption neither on the underlying high-scale model nor on the SUSY-breaking pattern.

We survey representative pMSSM benchmarks which satisfy all major experimental constraints from direct collider searches, flavor physics and electroweak precision data. All of them predict a Higgs boson mass of $m_h \simeq 126$ GeV and a LSP relic density close to the observed $\Omega h^2 = 0.1126 \pm 0.0036$. Specifically, we consider the following scenarios: Model 401479, 1889214, 2178683, 2342344, and 2948967, in the notation of Ref. [46]. Since the stop and sbottom masses range around 1 TeV we find pair production rates barely reaching $\mathcal{O}(1)$ fb at the topmost, with typical quantum effects ranging $K = 1.5 - 2$ for an LHC energy of 14 TeV. To study light stop and sbottom production we consider more specific scenarios:

a. Natural SUSY: Natural SUSY (NSUSY) features soft-breaking squark masses inversely proportional to their Higgs couplings, combined with a small Higgsino mass term [6]. Typical mass spectra feature sub-TeV heavy-flavor squarks, weak-scale higgsino-like neutralinos and charginos, and multi-TeV gluinos. We first examine two NSUSY scenarios [7] marked as ‘NSUSY1’ and ‘NSUSY2’ in Table I.

b. Natural-like constrained MSSM: Complementary NSUSY benchmarks follow Ref. [8]. We start from constrained MSSM (CMSSM) points [47] and assume non-universal squark soft-breaking masses at the GUT scale, leading to light third generation squarks, while the first and second generation stay above 1 TeV. The resulting CMSSM scenarios are labelled as ‘NS-CMSSM#’ in Table I.

c. Light SUSY: Finally, we consider configurations defined in Ref. [10]. They are not linked to GUT-scale assumptions but inspired by their implications on Higgs physics. For all scenarios we employ SOFTSUSY [48] to compute the physical particle masses.

	$m_{\tilde{t}_1}$	$m_{\tilde{t}_2}$	$m_{\tilde{b}_1}$	$m_{\tilde{b}_2}$	$m_{\tilde{u}_{L/R}}$	$m_{\tilde{d}_{L/R}}$	$m_{\tilde{g}}$	$m_{\tilde{\chi}_1^\pm}$	$m_{\tilde{\chi}_1^0}$
a. NSUSY 1	434.9	990.3	891.6	1356.9	13453/13444	13453/13444	3202.6	222.6	216.8
NSUSY 2	874.4	1614.4	1580.8	1969.9	7389.6/7381.1	7389.8/7361.1	2770.0	151.9	146.0
b. NS-CMSSM 10.2.2	398.4	682.5	572.4	684.6	5075.1/5071.7	5075.6/5071.7	1354.7	425.4	231.3
NS-CMSSM 40.2.2	255.8	611.8	471.5	649.8	5055.8/5054.2	5056.2/5054.1	1251.8	398.7	211.9
NS-CMSSM 40.3.2	320.0	610.9	528.3	771.7	5015.5/5017.6	5015.9/5017.9	974.6	288.6	157.1
c. Light SUSY	374.4	2022.9	387.9	2011.6	2013.2/2011.8	2014.6/2011.6	1102.3	498.9	301.3

Table I: Sparticle masses (in GeV) for the different MSSM benchmarks employed in our calculation.

III. RESULTS

In the stop–chargino sector the pair production of stop pairs and of a stop in association with a chargino are tied together, because at the NLO their on–shell and off–shell contributions overlap. We start by largely reviewing stop (and sbottom) pair production with a focus on light states and on their kinematic distributions. Then we move on the associated production process, which given the overwhelming backgrounds to chargino pair production might well be the most promising signature for charginos at the LHC.

A. Stop and sbottom pair production

We first compute the cross sections for the pair production of heavy–flavor squarks:

$$pp \rightarrow \tilde{t}_1 \tilde{t}_1^*, \tilde{b}_1 \tilde{b}_1^*. \quad (1)$$

The global K factor is defined as $K \equiv \sigma^{\text{NLO}}/\sigma^{\text{LO}}$. Some corresponding Feynman diagrams are displayed in Figure 1. At variance with the first and second generation squark production, the flavor–locked $q\bar{q}$ -initiated diagram with a gluino exchange is absent for stop pairs. For sbottom pairs, this diagram arises from the initial–state bottom quarks, which we include consistently in the five flavor scheme (5FS). We evaluate all rates for an LHC energy of 14 TeV. Representative MSSM parameter space regions are covered by the benchmark points defined in Section II. Unlike in PROSPINO the general setup of MADGOLEM enables us to separate all squark flavor and chirality without making assumptions on the mass spectrum.

Table II shows cross sections ranging from 10 fb to 10^4 fb for stop and sbottom masses up to the TeV range. The relative NLO correction is comparably stable at $K \sim 1.5 - 1.9$. This reflects the fact that the dominant NLO quantum effects arise from QCD, while SUSY-QCD corrections are subleading. The very slightly larger K factors for sbottom pair production compared to their stop counterparts are related to the additional one-loop effects from the gluino t -channel exchange between the incoming bottom partons. It is also illustrative to compare the rates to their light–flavor counterparts given in Table 2 of Ref. [31]. Novel one-loop contributions for example from non-diagonal $\tilde{q}_1 - \tilde{q}_2$ mixing self-energies are intrinsically tied to the heavy-flavor squark structure and account for the larger K -factors.

The automated MADGOLEM setup also provides predictions beyond total rates through the output of weighted event samples for the regularized virtual and real correction channels. They can be used to plot any NLO distribution

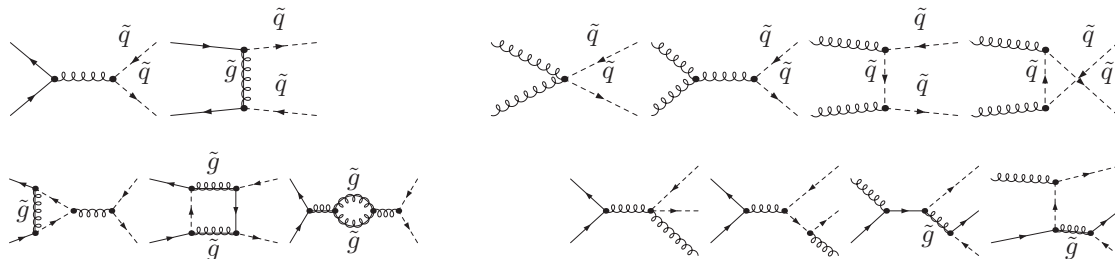


Figure 1: Feynman diagrams for squark–antisquark production at LO and at NLO. In the upper row we separately show quark and gluon initial states. The gluino exchange only features for sbottom pairs. For NLO we display representative vertex, box, and self-energy topologies as well as real corrections.

		$pp \rightarrow \tilde{t}_1 \tilde{t}_1^*$				$pp \rightarrow \tilde{b}_1 \tilde{b}_1^*$			
		$m_{\tilde{t}_1}$ [GeV]	σ^{LO} [fb]	σ^{NLO} [fb]	K	$m_{\tilde{b}_1}$ [GeV]	σ^{LO} [fb]	σ^{NLO} [fb]	K
a.	NSUSY 1	434.9	881	1380	1.57	891.6	10.6	18.0	1.70
	NSUSY 2	874.4	12.1	20.4	1.69	1580.8	0.11	0.23	1.87
b.	NS-CMSSM 10.2.2	398.4	1430	2210	1.54	572.4	180	290	1.61
	NS-CMSSM 40.2.2	255.8	14800	21800	1.47	471.5	558	882	1.58
	NS-CMSSM 40.3.2	320.0	4680	7010	1.50	528.3	28900	46200	1.60
c.	Light SUSY	374.4	2010	3080	1.53	387.9	1660	2550	1.53

Table II: Total rates and corresponding K factors for third generation squark pair production at the 14 TeV LHC.

which is consistently defined in perturbative QCD. In Figure 2 we display the distributions of the stop and sbottom transverse momentum and rapidity, including their scale uncertainties. As a representative MSSM configuration we choose NSUSY1 as defined in Table I. The distributions are normalized to unity for the central scale choice μ^0 ; the uncertainty envelope is generated through a parallel change of the renormalization and factorization scales in the conventional range $\mu^0/2 - 2\mu^0$. The transverse momentum of the stops has a strong peak slightly below 200 GeV. The fact that the lightest sbottom in this scenario is roughly twice as heavy as the stop explains why the sbottom distributions show a significantly harder and more central profile.

The stabilization of the (unphysical) scale dependence, which shrinks from $\mathcal{O}(60\%)$ at LO down to $\mathcal{O}(30\%)$ at NLO, reflects the improved precision of the higher order computation. The lower panels in Figure 2 show the corresponding K factors, also with their scale uncertainty. Its sizeable variation shows that the higher-order corrections cannot simply be described by a constant K factor. While in the past the LHC analyses would typically rely on central threshold production of heavy particles, more targeted analyses for example for light stops will be sensitive to specific phase space regions. In the case of stop pairs the K factor at threshold ranges around 1.7 ± 0.3 ; transverse stop momenta in the 300 GeV range still leave a sizeable fraction of events, but with a K factor around 1.6. While this effect is not dramatic given the quoted NLO error bars, it should be considered once we include higher order corrections.

In addition to the fixed-order NLO results in Figure 2 we also show the tree-level multi-jet merging results. For the latter we include up to two additional hard jets combined with the PYTHIA [49] parton shower and merge them via the MLM scheme [50] in MADGRAPH5 [51]. We consider three setups: i) up to one hard (gluon) jet; ii) up to two hard (gluon) jets; iii) up to one hard (light quark and gluon) jet. The first two approaches avoid any potential issues with on-shell singularities, which means they are only sensitive to QCD radiation. The third case involves a subset of bottom-initiated contributions which are sensitive to an intermediate on-shell gluino, just like the case shown in Figure 1. To improve speed we regularize this divergence by means of a numerical recipe implemented in MADGRAPH [34], which subtracts all events close to on-shell poles. While this subtraction method is not equivalent to the rigorous PROSPINO scheme and does not provide a well-defined zero-width limit, we have checked that it

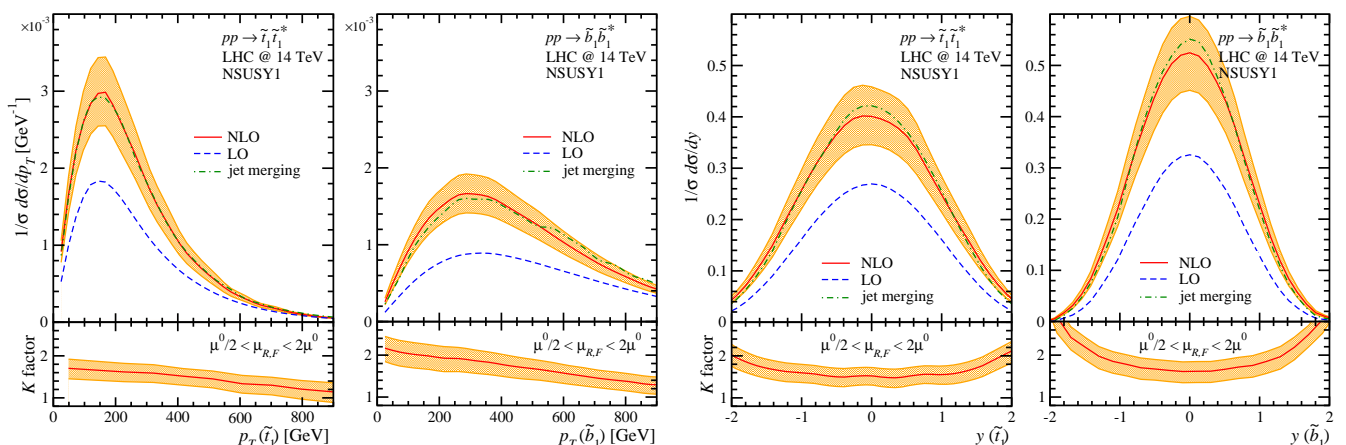


Figure 2: Normalized fixed-order NLO and tree-level merged distributions for $pp \rightarrow \tilde{t}_1 \tilde{t}_1^* / \tilde{b}_1 \tilde{b}_1^*$ as a function of the transverse momentum and rapidity. All MSSM parameters are fixed to the NSUSY1 benchmark in Table I. The error band for the NLO distributions corresponds to a variation $\mu^0/2 < \mu_{R,F} < 2\mu^0$. The lower panels show the corresponding K factors.

gives numerically similar results, as long as we consider normalized distributions².

This way we find that all three-jet merging setups agree very well with each other and with the fixed-order NLO result. Neither including a second hard gluon jet nor a light quark hard jet leads to any significant difference compared to the emission of up to one gluon. The observed shift towards slightly harder and more central squarks in the merged sample can be attributed to the additional recoil jets. All this is a common feature in the production of heavy colored resonances, which is characterized by a single hard scale well above the typical jet momenta required by inclusive searches [51, 52]. The same behavior can be seen in light-flavor squark and gluino production [31]. Once the double counting from the on-shell states is removed, the NLO real emission almost entirely consists of soft and collinear gluons, properly accounted for by the parton shower. As a note of caution we nonetheless keep in mind that once an experimental analysis becomes sensitive to the jet recoil the simulation should include matrix element and parton shower merging [53]. Examples for that are mono-jets searches as well as the analysis of forward (tagging) jets in the top/stop pair sample.

B. Associated stop–chargino production

Next, we consider top squark production in association with the lightest chargino,

$$pp \rightarrow \tilde{t}_1 \tilde{\chi}_1^- . \quad (2)$$

The LO process is flavor-locked, meaning that at parton level it relies on an incoming bottom quark. Throughout our calculation we resort to a five flavor scheme and use consistent parton densities and their corresponding α_s values. One technical caveat is that a massless bottom quark is incompatible with the left–right mixing in the sbottom sector. We circumvent this problem by assuming massless external bottom lines and propagators, while keeping a finite Yukawa coupling. The renormalization of the (massless) bottom quark and the (massive) bottom Yukawa is described in the Appendix. Further considerations on the flavor scheme choice are addressed in detail in subsection III C below.

As usual, NLO corrections proceed via virtual QCD and SUSY-QCD contributions and real emission. The relevant Feynman diagrams are illustrated in Figure 3. When we include bottom densities the perturbative counting requires some care, in particular for the genuine next-to-leading contributions which are no more flavor-locked. For example, off-shell stop pair production in quark–antiquark scattering or gluon fusion with a subsequent stop decay into a chargino contributes to the NLO rate. Strictly speaking, these diagrams are suppressed by one power of α_{EW} compared to the associate production at LO in the 5FS. On the other hand, modulo large logarithms the bottom density can be considered subleading to the gluon density by one power of α_s , in particular when the resummed logarithms are only moderately large. This means that we have to rely on other effects, like the size of off-shell vs on-shell contribution to ensure the perturbative stability of the rate predictions. Obviously, these complications will not be reflected in the scale variation as a measure of the theoretical uncertainty.

In addition, the real emission includes gluon splitting into a pair of bottoms in the initial state; this is the same diagram which defines the bottom parton densities in the collinear limit. However, as for any initial state, this collinear divergence is absorbed in the parton densities. In that sense the NLO computation in the 5FS can be viewed as the leading combination of the 4-flavor and the 5-flavor predictions [54]. The relative size of the two contributions

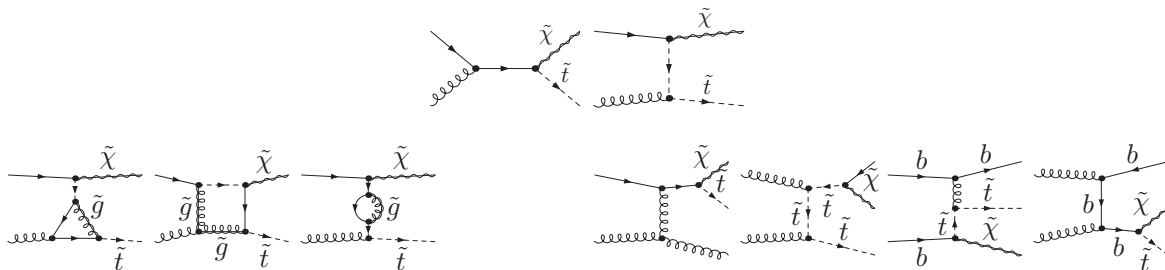


Figure 3: Feynman diagrams for the production of a top squark associated with a chargino at LO and at NLO. For the NLO case we show representative vertex, box, and self-energy topologies, as well as real corrections.

² For predictions of general distributions including the proper normalization only the PROSPINO scheme for on-shell subtraction will be consistent and numerically reliable.

		$m_{\tilde{t}_1}$ [GeV]	$m_{\tilde{\chi}_1^\pm}$ [GeV]	$pp \rightarrow \tilde{t}_1 \tilde{\chi}_1^-$ σ^{LO} [fb]	σ^{NLO} [fb]	K
a.	NSUSY1	434.9	222.6	40.97	49.98	1.22
	NSUSY2	874.4	151.9	1.94	2.51	1.29
b.	NSCMSSM-10.2.2	398.4	425.4	13.40	20.14	1.50
	NSCMSSM-40.2.2	255.8	398.7	47.83	71.21	1.48
	NSCMSSM-40.3.2	320.0	288.6	53.39	78.94	1.48
c.	Light SUSY	374.4	498.9	9.96	10.51	1.05

Table III: Total rates and corresponding K factors for single stop production associated with the lightest chargino at the 14 TeV LHC.

can be adjusted by varying the bottom factorization scale, as described in the following section. As discussed in the next section we use the average heavy mass of the final state as central renormalization and factorization scale.

We first use MADGOLEM to compute the total rates for stop–chargino production for the representative MSSM benchmarks defined in Table I. The results are documented in Table III. The rates can be as large as 80 fb and show tempered quantum effects $K \sim 1.1 - 1.5$, typically below their first-generation squark counterparts [30]. The main reason for the moderate quantum corrections are the smaller bottom luminosities, which suppress flavor–locked contributions $pp(bb) \rightarrow \tilde{t}_1 \tilde{\chi}_1^- b$ (cf. second diagram from the right in Figure 3) as compared to e.g. $pp(dd) \rightarrow \tilde{u}_L \tilde{\chi}_1^- d$. The different K -factors can be basically attributed to the relative sizes of the couplings $\tilde{t}_{1,2} \tilde{\chi}_1^\pm b$ in each scenario.

In Figure 4 we display the change of the total stop–chargino rates under correlated and independent variations of the renormalization and factorization scales. These scales are varied in the range $\mu^0/4 < \mu_{R,F} < 4\mu^0$ and follow the path illustrate in the little square of the first panel. In spite of its semi–weak nature, $\sigma^{\text{LO}} \propto \alpha_{EW} \alpha_s$, the scale dependence in this process is dominated by the renormalization scale. The fairly flat slope around the central scale, which for NSUSY1 reads $\mu^0 = (m_{\tilde{t}_1} + m_{\tilde{\chi}_1^\pm})/2 \simeq 328$ GeV, can be traced back to the individual scale dependence of the different parton densities. The valence quark, gluon and bottom densities largely balance each other and lead to an accidentally small factorization scale uncertainty. The renormalization scale variation corresponding to one power of the strong coupling does not reflect any of the complications associated with the perturbative series of this process, as discussed above. This means that we cannot expect the usual scale variation in the range $\mu^0/2 - 2\mu^0$ to provide a reliable estimate of the theoretical uncertainty. Correspondingly, the improvement of the scale dependence when including the NLO corrections in Figure 4 is rather limited.

Going beyond the total rates we show the differential distributions in the stop transverse momentum and rapidity, together with the multi–jet merging results in the 5FS in Figure 5. We find excellent agreement between the fixed–order and the jet merging calculations, the latter featuring as usual slightly harder, more central stops. As for the total rates, some of the key aspect of the NLO corrections are not governed by the scale dependence, which means that unlike for stop pair production the predictions from jet merging are not covered by the NLO scale dependence.

In Figure 6 we show in addition the transverse momentum distributions for the stop and for the chargino without subtracting stop pair production (denoted as $\tilde{t}_1 \tilde{t}_1^*$). For stop pair production the kinematics of the chargino are determined by the on–shell stop decays, and it is by accident that the transverse momentum distribution agrees with the associated production. In contrast, the transverse momentum of the stop should now be identical to Figure 2. While in associated production channel the transverse momentum of the stop peaks at low values slightly above

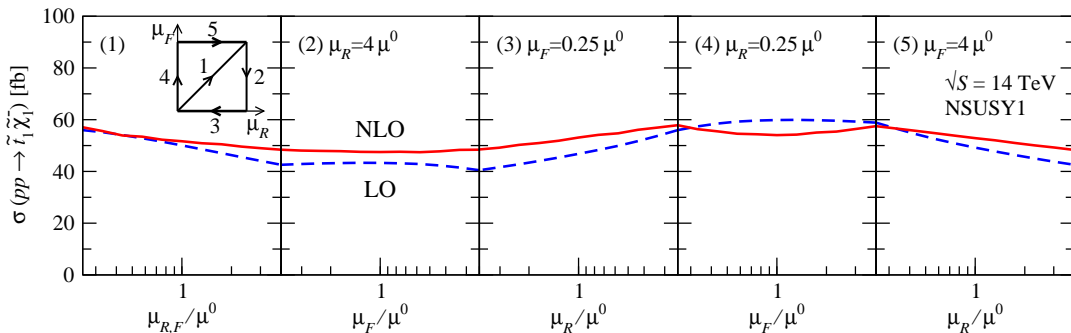


Figure 4: Fixed–order rates for stop production associated with the lightest chargino. We show the scale variation in the $\mu_R - \mu_F$ plane around the central scale $\mu^0 = (m_{\tilde{t}_1} + m_{\tilde{\chi}_1^\pm})/2$.

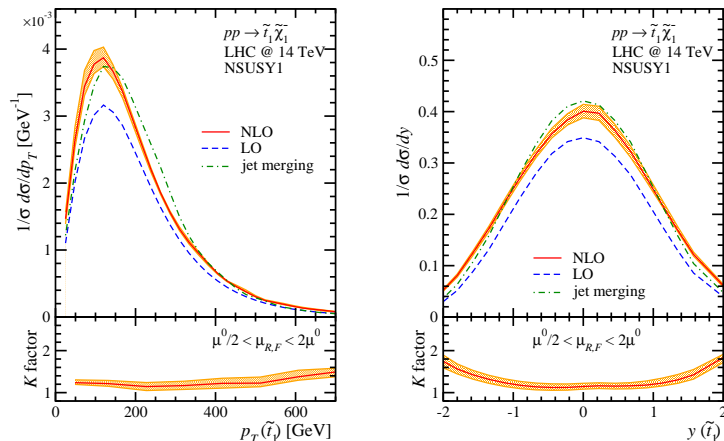


Figure 5: Normalized fixed-order NLO and tree-level merged distributions for $pp \rightarrow \tilde{t}_1 \tilde{\chi}_1^-$ as a function of the stop transverse momentum and rapidity. All MSSM parameters are fixed to the NSUSY1 benchmark in Table I. The error band for the NLO distributions corresponds to a variation $\mu^0/2 < \mu_{R,F} < 2\mu^0$. The lower panels show the corresponding K factors.

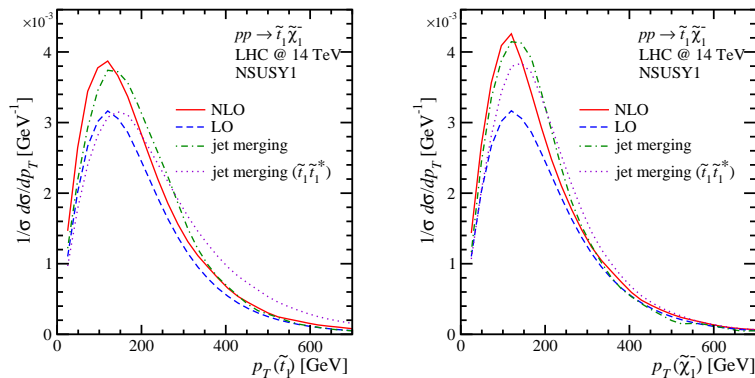


Figure 6: Normalized distributions for $pp \rightarrow \tilde{t}_1 \tilde{\chi}_1^-$ as a function of the stop and chargino transverse momentum. We compare the tree-level merged distributions retaining (dotted lines) and subtracting (dotted-dashed lines) stop pair production.

100 GeV, for stop pairs the peak increases by almost 200 GeV. The reason for this shift is that the incoming bottom-gluon system is significantly softer than a mix of incoming gluon-gluon or quark-antiquark pairs. When combining the two production channels at NLO the PROSPINO scheme for the on-shell subtraction allows for simply adding the two event samples correctly keeping track of these distinct features.

C. 4-flavor versus 5-flavor schemes

Owing to its flavor-locked nature, the associated production of heavy-flavor squarks relies on initial-state bottoms. This is exactly the same situation as for the associated production of a top quark with a charged Higgs boson [54]. Depending on the relevant scales and observables of interest such processes can be described either in a so-called 4-flavor (4FS) or a 5-flavor scheme (5FS) [54–56].

In the 4FS bottom quarks are not considered partons inside the proton, but they are generated dynamically via gluon splitting as part of the hard process. The bottom mass acts as an infrared regulator for inclusive observables, which means that the numerical predictions are reliable as long as m_b is not too different from the relevant scales of the process. One advantage of this scheme is that it retains the full bottom-mass dependence in the final state kinematics.

The production of massive states with comparably low transverse momenta in the gluon splitting will be dominated by collinear gluon splitting. The bottom mass still acts as a mathematical cutoff, but it also generates a large physical logarithm, so the final-state bottom jets peak at large rapidity, $y_b \simeq 2$, and low transverse momenta, $p_{T,b} \simeq m_b$. In this kinematic regime the b -tagging becomes a challenge, so the experimentally relevant observables do not include

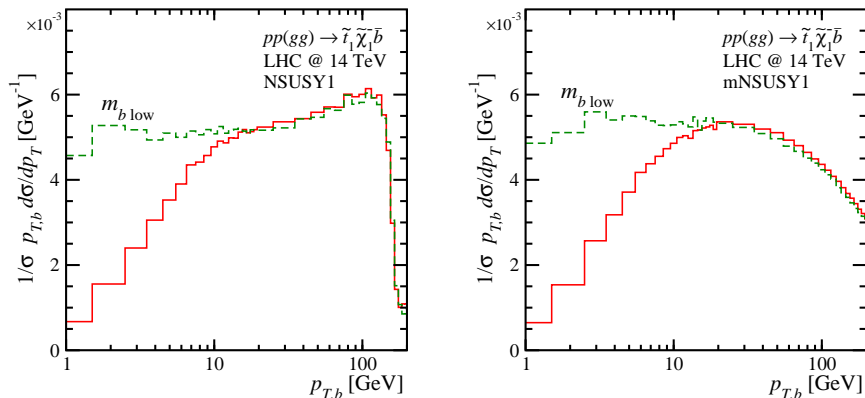


Figure 7: Distributions $p_{T,b} d\sigma/dp_{T,b}$ for the process $pp(gg) \rightarrow \tilde{t}_1 \tilde{\chi}_1^- \bar{b}$ at the 14 TeV LHC. We examine different MSSM benchmarks separately, as described in the text. The (m)NSUSY1 scenario with a low bottom mass, $m_{b,\text{low}} = m_b/10$, is also shown by a dotted line as a reference.

the bottom radiation. To predict the bottom-inclusive rate we need to integrate over the phase space of the bottom radiation, approaching the asymptotic form

$$\frac{d\sigma[\tilde{t}_1 \tilde{\chi}_1^- \bar{b}]}{dp_{T,b}} \sim \frac{p_{T,b}}{p_{T,b}^2 + m_b^2} \quad \text{and hence} \quad \sigma[\tilde{t}_1 \tilde{\chi}_1^- \bar{b}] \sim \log \frac{p_{T,b}^{\text{max}}}{m_b}. \quad (3)$$

This potentially large logarithm is the same logarithm which appears in any QCD splitting regularized by a finite quark mass [55]. Its resummation can be linked to introducing a scale-dependent bottom parton density for the inclusive process $gb \rightarrow \tilde{t}_1 \tilde{\chi}_1^-$, defining the 5FS. This link identifies $p_{T,b}^{\text{max}}$ with the factorization scale of the bottom parton, implying that such scale is not a free parameter, but can be computed from the kinematics of the splitting process which generates the bottom parton density. Usually, in this approach the now incoming bottom parton is assumed to be massless, but mass corrections can be included in the parton splittings [55].

The 5FS is hence justified as long as we do not reconstruct the final-state bottom jet and as long as the bottom mass is negligible compared to the hard scale of the process. While it is easy to show that the factorization scale is linear with the hard scale, $\mu_{F,b} \propto m_1 + m_2$, the associated prefactor is process dependent. For example, the bottom factorization scale for a leading bq initial state should be larger than for a bg initial state, because incoming gluons carry less momentum to generate hard radiation than incoming quarks. The link between the improved perturbative prediction and the appropriate scale choice has been thoroughly studied in the context of Higgs production [54, 57].

In the following we validate the 5-flavor approach, as applied in the previous Section III B, by analyzing the bottom jet kinematics in the 4FS [54]. As representative benchmark points, we choose the NSUSY1 scenario defined in Table I and the modified NSUSY1 (mNSUSY1) setup, which differs from the original NSUSY1 parameter point in the heavier chargino mass $m_{\tilde{\chi}_1^\pm} = 1$ TeV. The latter avoids resonant stop decays and the associated on-shell resonances. Here we use the NNPDF21_FFNNF4.100 [44] parton density with four active flavors and a bottom mass fixed to $m_b = 4.78$ GeV.

We show the transverse momentum distribution of the radiated bottom quark in Figure 7, normalizing it such that a flat behavior corresponds to the proper asymptotic scaling shown in Eq.(3). For the regular parameter point the distribution has dropped to half of its plateau value for $p_{T,b} \sim 200$ GeV, while for the heavier chargino the distribution extends to significantly larger transverse momenta. A factorization scale $\mu_{F,b} = (m_1 + m_2)/2$ appears fully justified by these results, if we extend the uncertainty band to sufficiently low factorization scales.

IV. SUMMARY

In the upcoming LHC runs dedicated searches for light stops, possibly in association with light charginos, will play an increasingly important role. This requires a precise understanding of the production processes in perturbative QCD. We have studied the pair production and the associated production of heavy-flavor squarks in the automated MADGOLEM framework. For a set of representative up-to-date MSSM parameter points with light stops and sbottoms we have examined the total and differential production rates to NLO accuracy. We find that

- for stop and sbottom pair production the K factors range around 1.5–1.9, with significant variations over phase space. For the associated stop–chargino case, we find comparably constant corrections around $K = 1.1 - 1.5$.

In both cases there exists a K factor variation over phase space, which might require NLO distributions for some phase space regions.

- these corrections are mainly due to QCD radiation, whilst SUSY-QCD corrections are subleading. The NLO distributions agree well with predictions from up to two additional jets merged from the matrix element and the parton shower.
- the bottom-inclusive or 5-flavor picture is suitable for stop-chargino production, with a bottom factorization scale around the average mass of the two heavy states.
- unlike for stop pairs, the scale dependence of the associated production channel cannot be used as a conservative measure of the theory uncertainties.

Aside from the already built-in MADGOLEM functionalities, such as the automated UV renormalization, SUSY dipoles and on-shell subtraction, the current version has been upgraded to support squark mixing, the associated counter terms, and finite quark mass effects. This completes the MADGOLEM program.

Acknowledgments

It is a pleasure to thank Juan Rojo and Maria Ubiali for kindly providing us a leading-order version of the NNPDF21.FFN.NF4 parton densities as well as for enlightening discussions. This work is supported in part by the Belgian Federal Science Policy Office through the Interuniversity Attraction Pole P7/37. DLV is funded by the F.R.S.-FNRS *Fonds de la Recherche Scientifique* (Belgium). KM is supported by the Strategic Research Program *High Energy Physics* and the Research Council of the Vrije Universiteit Brussel.

Appendix A: Renormalization

In this appendix we summarize the aspects of the general MSSM renormalization relevant for SUSY-QCD interactions involving third generation squarks. For a comprehensive account on the notation setup and the technical implementation in MADGOLEM we refer the reader to the dedicated appendices of Ref. [31].

The renormalization of the MSSM heavy flavor squarks has been addressed extensively. The problem was first tackled in the context of squark decays and was extended later on for squark pair production [58]; and radiative corrections to the MSSM Higgs boson masses [61]. Renormalization scheme issues have been examined in detail in Refs. [62–64].

Leading order parameterization

Let us consider the squark kinetic term within the general MSSM Lagrangian,

$$\mathcal{L} = \sum_{\tilde{q}=\tilde{t},\tilde{b}} (\partial_\mu \tilde{q}_L^* \partial_\mu \tilde{q}_R) \begin{pmatrix} \partial^\mu \tilde{q}_L \\ \partial^\mu \tilde{q}_R \end{pmatrix} - (\tilde{q}_L^* \tilde{q}_R^*) \mathcal{M}_{\tilde{q}}^2 \begin{pmatrix} \tilde{q}_L \\ \tilde{q}_R \end{pmatrix}, \quad (\text{A1})$$

with the mass-squared matrix,

$$\mathcal{M}_{\tilde{q}}^2 = \begin{pmatrix} M_{\tilde{q}_L}^2 + m_q^2 + m_Z^2 (T_{3,q} - Q_q s_W^2) \cos 2\beta & m_q X_q \\ m_q X_q & M_{\tilde{q}_R}^2 + m_q^2 + m_Z^2 Q_q s_W^2 \cos 2\beta \end{pmatrix}. \quad (\text{A2})$$

Following standard conventions, we introduce $X_q \equiv A_q - \mu \{\cot \beta, \tan \beta\}$ with $\{\cot \beta, \tan \beta\}$ related to $\{t, b\}$ respectively. This parameter is connected to the vacuum expectation values of the two MSSM Higgs doublet fields, $\tan \beta \equiv v_2/v_1$. The squark mass terms $M_{\tilde{q}_{L(R)}}^2$ and the trilinear coupling A_q define the relevant soft-SUSY breaking parameters; μ represents the supersymmetric Higgsino mass term; and $m_q, Q_q, T_{3,q}$ stand for the (heavy) quark mass, electric charge and third component weak isospin.

The symmetric mass matrix in Eq.(A2) is diagonalized through the unitary transformation $R^{\tilde{q}} \equiv R(\theta_{\tilde{q}})$ which rotates the squark gauge eigenstates $\tilde{q}_{L(R)}$ into the physical squark basis $\tilde{q}_{1(2)}$. The squark mass eigenvalues $m_{\tilde{q}_{1(2)}}$ and the mixing angle $\theta_{\tilde{q}}$ can thus be expressed in terms of the MSSM input parameters, cf. e.g. [59].

Renormalization scheme

The required vertex counterterms are generated by multiplicative renormalization of the respective wave functions and model parameters,

$$\Psi^{(0)} \rightarrow Z_\Psi^{1/2} \Psi, \quad m_\Psi^{(0)} \rightarrow m_\Psi + \delta m_\Psi, \quad g_s^{(0)} \rightarrow g_s + \delta g_s. \quad (\text{A3})$$

In line with this general procedure, we replace the bare squark field and squark mass matrices by their respective renormalized expressions,

$$\begin{aligned} \begin{pmatrix} \tilde{q}_1 \\ \tilde{q}_2 \end{pmatrix} &\rightarrow (R^{\tilde{q}}) \left[\mathbb{1}_{2 \times 2} + \frac{1}{2} \delta Z^{\tilde{q}} \right] \begin{pmatrix} \tilde{q}_L \\ \tilde{q}_R \end{pmatrix} \quad \text{with} \quad \delta Z^{\tilde{q}} = \begin{pmatrix} \delta Z_{\tilde{q}_1}^{\tilde{q}} & \delta Z_{12}^{\tilde{q}} \\ \delta Z_{21}^{\tilde{q}} & \delta Z_{\tilde{q}_2}^{\tilde{q}} \end{pmatrix}, \\ R^{\tilde{q}} \mathcal{M}_{\tilde{q}}^2 (R^{\tilde{q}})^\dagger &\rightarrow R^{\tilde{q}} \mathcal{M}_{\tilde{q}}^2 (R^{\tilde{q}})^\dagger + R^{\tilde{q}} \delta \mathcal{M}_{\tilde{q}}^2 (R^{\tilde{q}})^\dagger = \begin{pmatrix} m_{\tilde{q}_1}^2 & 0 \\ 0 & m_{\tilde{q}_2}^2 \end{pmatrix} + \begin{pmatrix} \delta m_{\tilde{q}_1}^2 & \delta Y_{\tilde{q}}^2 \\ \delta Y_{\tilde{q}}^2 & \delta m_{\tilde{q}_2}^2 \end{pmatrix}, \end{aligned} \quad (\text{A4})$$

where $\delta Y_{\tilde{q}}^2 \equiv (m_{\tilde{q}_1}^2 - m_{\tilde{q}_2}^2) \delta \theta_{\tilde{q}}$. Expanding the squark kinetic term of Eq.(A1) gives for each of the squarks

$$\delta \mathcal{L} = \frac{1}{2} (\partial_\mu \tilde{q}_1^*, \partial_\mu \tilde{q}_2^*) (\delta Z^{\tilde{q}\dagger} + \delta Z^{\tilde{q}}) \begin{pmatrix} \partial^\mu \tilde{q}_1 \\ \partial^\mu \tilde{q}_2 \end{pmatrix} - \frac{1}{2} (\tilde{q}_1^* \tilde{q}_2^*) \left[(\delta Z^{\tilde{q}\dagger} + \delta Z^{\tilde{q}}) \begin{pmatrix} m_{\tilde{q}_1}^2 & 0 \\ 0 & m_{\tilde{q}_2}^2 \end{pmatrix} + 2 \begin{pmatrix} \delta m_{\tilde{q}_1}^2 & \delta Y_{\tilde{q}}^2 \\ \delta Y_{\tilde{q}}^2 & \delta m_{\tilde{q}_2}^2 \end{pmatrix} \right] \begin{pmatrix} \tilde{q}_1 \\ \tilde{q}_2 \end{pmatrix}, \quad (\text{A5})$$

where from we can readily extract the coefficients of the (matrix-valued) renormalized squark self-energy:

$$\begin{aligned} \Re e \hat{\Sigma}_{\tilde{q}_a}^{\tilde{q}}(p^2) &= \Re e \Sigma_{\tilde{q}_a}^{\tilde{q}}(p^2) + \frac{1}{2} (\delta Z_{\tilde{q}_a}^{\tilde{q}} + \delta Z_{\tilde{q}_a}^{\tilde{q}\dagger}) (p^2 - m_{\tilde{q}_a}^2) - \delta m_{\tilde{q}_a}^2 \quad [a = 1, 2], \\ \Re e \hat{\Sigma}_{12}^{\tilde{q}}(p^2) &= \Re e \Sigma_{12}^{\tilde{q}}(p^2) + \frac{1}{2} \delta Z_{12}^{\tilde{q}} (p^2 - m_{\tilde{q}_1}^2) + \frac{1}{2} \delta Z_{21}^{\tilde{q}} (p^2 - m_{\tilde{q}_2}^2) - (\delta Y_{\tilde{q}}^2). \end{aligned} \quad (\text{A6})$$

As long as we limit ourselves to SUSY-QCD interactions, the top–stop system is fully characterized at one loop by four independent parameters, these are: the top quark mass m_t ; the top squark masses $m_{\tilde{t}_1}, m_{\tilde{t}_2}$; and the top squark mixing angle $\theta_{\tilde{t}}$. We fix the corresponding counterterms using generalized on–shell conditions [59, 60, 63] which, together with the mixed wave–function renormalization, absorb stop mixing in external legs³:

1. on-shell top quark mass

$$\Re e \hat{\Sigma}_{\tilde{t}}^{\tilde{t}}(m_t^2) = 0 \quad \rightarrow \quad \frac{\delta m_t}{m_t} = \frac{1}{2} [\Re e \Sigma_{\tilde{t}_L}^{\tilde{t}}(m_t^2) + \Re e \Sigma_{\tilde{t}_R}^{\tilde{t}}(m_t^2) + 2 \Re e \Sigma_{\tilde{t}_S}^{\tilde{t}}(m_t^2)], \quad (\text{A7})$$

where the conventional Lorenz decomposition of the fermionic self-energies reads

$$\Re e \Sigma_q(p^2) = \not{p} P_L \Re e \Sigma_{qL}(p^2) + \not{p} P_R \Re e \Sigma_{qR}(p^2) + m_f \Re e \Sigma_{qS}(p^2). \quad (\text{A8})$$

2. on-shell top squark masses ($a = 1, 2$)

$$\Re e \hat{\Sigma}_{\tilde{t}_a}^{\tilde{t}}(m_{\tilde{t}_a}^2) = 0 \quad \rightarrow \quad \delta m_{\tilde{t}_a}^2 = \Re e \Sigma_{\tilde{t}_a}^{\tilde{t}}(m_{\tilde{t}_a}^2). \quad (\text{A9})$$

3. no–mixing condition for on-shell stops

$$\Re e \hat{\Sigma}_{12}^{\tilde{t}}(m_{\tilde{t}_a}^2) = 0. \quad (\text{A10})$$

In view of Eq.(A6) the latter condition fixes the mixing angle counterterm $\theta_{\tilde{t}}$ as:

$$\delta \theta_{\tilde{t}} = \frac{1}{2} \frac{\Re e \Sigma_{12}^{\tilde{t}}(m_{\tilde{t}_1}^2) + \Re e \Sigma_{12}^{\tilde{t}}(m_{\tilde{t}_2}^2)}{m_{\tilde{t}_1}^2 - m_{\tilde{t}_2}^2} \quad \text{or} \quad \delta Y_{\tilde{t}}^2 = \frac{1}{2} [\Re e \Sigma_{12}^{\tilde{t}}(m_{\tilde{t}_1}^2) + \Re e \Sigma_{12}^{\tilde{t}}(m_{\tilde{t}_2}^2)]. \quad (\text{A11})$$

The non–diagonal field renormalization constants then read

$$\delta Z_{12}^{\tilde{t}} = \delta Z_{21}^{\tilde{t}} = \frac{\Re e \Sigma_{12}^{\tilde{t}}(m_{\tilde{t}_2}^2) - \Re e \Sigma_{12}^{\tilde{t}}(m_{\tilde{t}_1}^2)}{m_{\tilde{t}_1}^2 - m_{\tilde{t}_2}^2}. \quad (\text{A12})$$

³ Another possibility is to define a running mixing angle and fully diagonal wave functions [60].

4. Last, additional on-shell conditions fix the (diagonal) stop field renormalization constants ($a = 1, 2$)

$$\Re e \hat{\Sigma}'_{\tilde{t}_a}(p^2) \Big|_{p^2=m_{\tilde{t}_a}^2} = 0 \quad \rightarrow \quad \delta Z_{\tilde{t}_a} = -\Re e \Sigma'_{\tilde{t}_a}(m_{\tilde{t}_a}^2), \quad (\text{A13})$$

with the conventional shorthand notation $\Re e \Sigma' \equiv d^2/dp^2 \Re e \Sigma(p^2)$.

Similar on-shell conditions are used to renormalize the bottom-sbottom sector. The gauge link between the sbottom and stop sectors must be accounted for properly [63]. In practice, all input masses in MADGOLEM are defined on-shell. The physical on-shell squark masses for example from SOFTSUSY can then be used as input parameters consistent with the on-shell squark mass counterterms.

Renormalization constants

The different field and mass renormalization constants are derived from the one-loop self-energies involving the interchange of virtual gluons and gluinos. The strong coupling constant is renormalized in the $\overline{\text{MS}}$ scheme explicitly decoupling all particles heavier than the bottom quark. This zero-momentum subtraction scheme [23, 66, 67] leaves us with the renormalization group running of α_s from light colored particles only. It corresponds to the measured value of the strong coupling, for example in a combined fit with the parton densities. Its renormalization constant reads

$$\delta g_s = -\frac{\alpha_s}{4\pi} \frac{\beta_0^L + \beta_0^H}{2} \frac{1}{\tilde{\epsilon}} - \frac{\alpha_s}{4\pi} \left(\frac{1}{3} \log \frac{m_t^2}{\mu_R^2} + \log \frac{m_{\tilde{g}}^2}{\mu_R^2} + \frac{1}{12} \sum_{\text{squarks}} \log \frac{m_{\tilde{q}_a}^2}{\mu_R^2} \right). \quad (\text{A14})$$

The UV divergence appears as $1/\tilde{\epsilon} \equiv (4\pi)^\epsilon/\Gamma(1-\epsilon) = 1/\epsilon - \gamma_E + \log(4\pi) + \mathcal{O}(\epsilon)$. Both light (L) and heavy (H) colored particles contribute to the beta function

$$\beta_0 = \beta_0^L + \beta_0^H = \left[\frac{11}{3} C_A - \frac{2}{3} n_f \right] + \left[-\frac{2}{3} - \frac{2}{3} C_A - \frac{1}{3} (n_f + 1) \right]. \quad (\text{A15})$$

MADGOLEM sets the number of active flavors to $n_f = 5$. The $SU(3)_C$ color factors are $C_F = 4/3$ and $C_A = 3$.

In the case of the gluon field, the heavy colored particles are decoupled consistently with the 5-flavor scheme used for the strong coupling constant renormalization. The underlying Slavnov-Taylor identities relate the corresponding finite counterterms as $\delta Z_G = -2\delta g_s$. Explicit analytical expressions for the field and mass renormalization constants relevant for the processes considered in this paper are documented below. The results are given in terms of standard Passarino-Veltman scalar functions [68]

– (massive) quark field

$$\begin{aligned} \delta Z_{qL/R} = & \frac{\alpha_s C_F}{4\pi} \left\{ 1 + 4m_q^2 B'_0(m_q^2, 0, m_q^2) + 2m_{\tilde{g}} m_q \sin(2\theta_{\tilde{q}}) [B'_0(m_q^2, m_{\tilde{q}_1}^2, m_{\tilde{g}}^2) - B'_0(m_q^2, m_{\tilde{q}_2}^2, m_{\tilde{g}}^2)] \right. \\ & + \frac{\cos^2 \theta_{\tilde{q}} A_0(m_{\tilde{q}_1}^2) + \sin^2 \theta_{\tilde{q}} A_0(m_{\tilde{q}_2}^2) - A_0(m_q^2) - A_0(m_{\tilde{g}}^2)}{m_q^2} - \frac{m_{\tilde{q}_1}^2 - m_{\tilde{g}}^2}{m_q^2} B_0(m_q^2, m_{\tilde{g}}^2, m_{\tilde{q}_1}^2) \\ & - \frac{m_{\tilde{q}_2}^2 - m_{\tilde{g}}^2}{m_q^2} B_0(m_q^2, m_{\tilde{g}}^2, m_{\tilde{q}_2}^2) - (m_q^2 + m_{\tilde{g}}^2 - m_{\tilde{q}_1}^2) \left[B'_0(m_q^2, m_{\tilde{g}}^2, m_{\tilde{q}_1}^2) + \frac{\sin^2 \theta_{\tilde{q}}}{m_q^2} B_0(m_q^2, m_{\tilde{g}}^2, m_{\tilde{q}_1}^2) \right] \\ & \left. - (m_q^2 + m_{\tilde{g}}^2 - m_{\tilde{q}_2}^2) \left[B'_0(m_q^2, m_{\tilde{g}}^2, m_{\tilde{q}_2}^2) + \frac{\cos^2 \theta_{\tilde{q}}}{m_q^2} B_0(m_q^2, m_{\tilde{g}}^2, m_{\tilde{q}_2}^2) \right] \right\}. \quad (\text{A16}) \end{aligned}$$

– (massive) quark mass

$$\begin{aligned} \frac{\delta m_q}{m_q} = & -\frac{\alpha_s C_F}{8\pi m_q^2} \left\{ 2m_q^2 + 6A_0(m_q^2) + 2A_0(m_{\tilde{g}}^2) - A_0(m_{\tilde{q}_1}^2) - A_0(m_{\tilde{q}_2}^2) \right. \\ & - 2m_q m_{\tilde{g}} \sin(2\theta_{\tilde{q}}) [B_0(m_q^2, m_{\tilde{g}}^2, m_{\tilde{q}_2}^2) - B_0(m_q^2, m_{\tilde{g}}^2, m_{\tilde{q}_1}^2)] \\ & \left. - (m_q^2 - m_{\tilde{q}_1}^2 + m_{\tilde{g}}^2) B_0(m_q^2, m_{\tilde{g}}^2, m_{\tilde{q}_1}^2) - (m_q^2 - m_{\tilde{q}_2}^2 + m_{\tilde{g}}^2) B_0(m_q^2, m_{\tilde{g}}^2, m_{\tilde{q}_2}^2) \right\}. \quad (\text{A17}) \end{aligned}$$

– squark field (diagonal)

$$\begin{aligned} \delta Z_{\tilde{q}_1} = & -\frac{\alpha_s C_F}{2\pi} \left[B_0(m_{\tilde{q}}^2, m_q^2, m_{\tilde{g}}^2) - B_0(m_{\tilde{q}_1}^2, 0, m_{\tilde{q}_1}^2) \right. \\ & \left. + 2m_{\tilde{g}} m_q \sin(2\theta_{\tilde{q}}) B_0'(m_{\tilde{q}_1}^2, m_q^2, m_{\tilde{g}}^2) - (m_q^2 + m_{\tilde{g}}^2 - m_{\tilde{q}}^2) B_0'(m_{\tilde{q}_1}^2, m_q^2, m_{\tilde{g}}^2) - 2m_{\tilde{q}_1}^2 B_0'(m_{\tilde{q}_1}^2, 0, m_{\tilde{q}_1}^2) \right], \end{aligned} \quad (\text{A18})$$

and likewise for \tilde{q}_2 with $1 \rightarrow 2$ and $\theta_{\tilde{q}} \rightarrow -\theta_{\tilde{q}}$.

– squark field (mixing)

$$\delta Z_{12}^{\tilde{q}} = -\frac{\alpha_s C_F}{\pi} \frac{m_q m_{\tilde{g}}}{(m_{\tilde{q}_1}^2 - m_{\tilde{q}_2}^2)} \cos(2\theta_{\tilde{q}}) \left[B_0(m_{\tilde{q}_1}^2, m_q^2, m_{\tilde{g}}^2) - B_0(m_{\tilde{q}_2}^2, m_q^2, m_{\tilde{g}}^2) \right]. \quad (\text{A19})$$

– squark mixing angle

$$\delta \theta_{\tilde{q}} = \frac{\alpha_S C_F}{4\pi} \frac{\cos(2\theta_{\tilde{q}})}{m_{\tilde{q}_1}^2 - m_{\tilde{q}_2}^2} \left\{ 2m_b m_{\tilde{g}} \left[B_0(m_{\tilde{q}_1}^2, m_q^2, m_{\tilde{g}}^2) + B_0(m_{\tilde{q}_2}^2, m_q^2, m_{\tilde{g}}^2) \right] + \sin(2\theta_{\tilde{q}}) \left[A_0(m_{\tilde{q}_2}^2) - A_0(m_{\tilde{q}_1}^2) \right] \right\}. \quad (\text{A20})$$

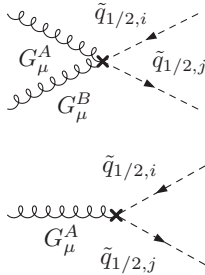
– squark mass

$$\begin{aligned} \delta m_{\tilde{q}_1}^2 = & -\frac{\alpha_s C_F}{4\pi} \left[4m_{\tilde{q}_1}^2 + 2A_0(m_q^2) + 2A_0(m_{\tilde{g}}^2) + 2A_0(m_{\tilde{q}_1}^2) + 2(m_{\tilde{g}}^2 - m_{\tilde{q}_1}^2 + m_q^2) B_0(m_{\tilde{q}_1}^2, m_{\tilde{g}}^2, m_q^2) \right. \\ & \left. - 4m_q m_{\tilde{g}} \sin(2\theta_{\tilde{q}}) B_0(m_{\tilde{q}_1}^2, m_{\tilde{g}}^2, m_q^2) + \sin^2(2\theta_{\tilde{q}}) (A_0(m_{\tilde{q}_1}^2) - A_0(m_{\tilde{q}_2}^2)) \right], \end{aligned} \quad (\text{A21})$$

and likewise for \tilde{q}_2 with $1 \rightarrow 2$ and $\theta_{\tilde{q}} \rightarrow -\theta_{\tilde{q}}$.

Counterterms

The strong interaction counter terms for squark pair production in the MSSM are given by:



$$\begin{aligned} & -i g_s T_{ij}^A \left[\delta g_s + \frac{\delta Z_{\tilde{q}_{1/2,i}} + \delta Z_{\tilde{q}_{1/2,j}} + \delta Z_G}{2} \right] \tilde{q}_{1/2,i} (p_i + p_j)^\mu G_\mu^A \tilde{q}_{1/2,j} \\ & i g_s^2 \{T^A T^B\}_{ij} \left[2\delta g_s + \delta Z_G + \frac{\delta Z_{\tilde{q}_{1/2,i}} + \delta Z_{\tilde{q}_{1/2,j}}}{2} \right] \tilde{q}_{1/2,i} \tilde{q}_{1/2,j} G_\mu^A G^{B\mu} \end{aligned}$$

The SUSY-electroweak interactions to leading order read

$$g_{\tilde{t}_a b \tilde{\chi}_i^-} = \tilde{t}_a \bar{b} \left(g_{\tilde{\chi}_i^- b, L}^{(1)} P_R + g_{\tilde{\chi}_i^- b, R}^{(2)} P_L \right) \tilde{\chi}_i^-, \quad g_{\tilde{t}_a b \tilde{\chi}_i^+} = \tilde{t}_a^* \tilde{\chi}_i^+ \left(g_{\tilde{\chi}_i^+ b, L}^{(1)} P_R + g_{\tilde{\chi}_i^+ b, R}^{(2)} P_L \right) b, \quad (\text{A22})$$

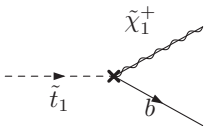
with coupling components

$$\begin{aligned} g_{\tilde{t}_1 b \tilde{\chi}_i^-}^{(a)} &= R_{11}^{\tilde{t}} g_{\tilde{\chi}_i^- b, L}^{(a)} + R_{12}^{\tilde{t}} g_{\tilde{\chi}_i^- b, R}^{(a)}, & g_{\tilde{t}_2 b \tilde{\chi}_i^-}^{(a)} &= R_{21}^{\tilde{t}} g_{\tilde{\chi}_i^- b, L}^{(a)} + R_{22}^{\tilde{t}} g_{\tilde{\chi}_i^- b, R}^{(a)}, \\ g_{\tilde{t}_1^* b \tilde{\chi}_i^+}^{(a)} &= R_{11}^{\tilde{t}} g_{\tilde{\chi}_i^+ b, L}^{(a)} + R_{12}^{\tilde{t}} g_{\tilde{\chi}_i^+ b, R}^{(a)}, & g_{\tilde{t}_2^* b \tilde{\chi}_i^+}^{(a)} &= R_{21}^{\tilde{t}} g_{\tilde{\chi}_i^+ b, L}^{(a)} + R_{22}^{\tilde{t}} g_{\tilde{\chi}_i^+ b, R}^{(a)} \quad (a = 1, 2), \end{aligned} \quad (\text{A23})$$

and

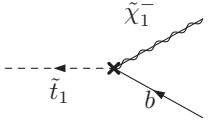
$$\begin{aligned} g_{\tilde{\chi}_i^- b, L}^{(1)} &= g_{\tilde{\chi}_i^+ b, L}^{(2)} = \frac{-eV_{11}}{s_W}, & g_{\tilde{\chi}_i^- b, L}^{(2)} &= g_{\tilde{\chi}_i^+ b, L}^{(1)} = \frac{em_b U_{12}}{\sqrt{2} s_W m_W \cos \beta}, \\ g_{\tilde{\chi}_i^- b, R}^{(1)} &= g_{\tilde{\chi}_i^+ b, R}^{(2)} = \frac{em_t V_{12}}{\sqrt{2} s_W m_W \sin \beta}, & g_{\tilde{\chi}_i^- b, R}^{(2)} &= g_{\tilde{\chi}_i^+ b, R}^{(1)} = 0. \end{aligned} \quad (\text{A24})$$

in terms of the chargino mixing matrices U and V . The finite SUSY-restoring counterterm $\delta_{\text{SUSY}} = -\alpha_s/(6\pi)$ corrects the mismatch of two gaugino and the $2-2\epsilon$ degrees of freedom induced by the use of dimensional regularization. The corresponding counter terms are



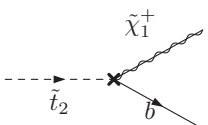
$$\delta[g_{\tilde{t}_1 b \tilde{\chi}_i^-}^{(1)}] = g_{\tilde{t}_1 \tilde{\chi}_i^- b, L}^{(1)} \left[R_{11}^{\tilde{t}} \left(\frac{\delta Z_{b_L}^\dagger + \delta Z_{\tilde{t}_1}}{2} + \delta_{\text{SUSY}} \right) + R_{21}^{\tilde{t}} \frac{\delta Z_{12}^{\tilde{t}}}{2} \right] + g_{\tilde{t}_1 \tilde{\chi}_i^- b, R}^{(1)} \left[R_{12}^{\tilde{t}} \left(\frac{\delta Z_{b_L}^\dagger + \delta Z_{\tilde{t}_1}}{2} + \frac{\delta m_t}{m_t} + \delta_{\text{SUSY}} \right) + R_{22}^{\tilde{t}} \frac{\delta Z_{12}^{\tilde{t}}}{2} \right]$$

$$\delta[g_{\tilde{t}_1 b \tilde{\chi}_i^-}^{(2)}] = g_{\tilde{t}_1 \tilde{\chi}_i^- b, L}^{(2)} \left[R_{11}^{\tilde{t}} \left(\frac{\delta Z_{b_R}^\dagger + \delta Z_{\tilde{t}_1}}{2} + \frac{\delta m_b}{m_b} + \delta_{\text{SUSY}} \right) + R_{21}^{\tilde{t}} \frac{\delta Z_{12}^{\tilde{t}}}{2} \right] + g_{\tilde{t}_1 \tilde{\chi}_i^- b, R}^{(2)} \left[R_{12}^{\tilde{t}} \left(\frac{\delta Z_{b_R}^\dagger + \delta Z_{\tilde{t}_1}}{2} + \delta_{\text{SUSY}} \right) + R_{22}^{\tilde{t}} \frac{\delta Z_{12}^{\tilde{t}}}{2} \right]$$



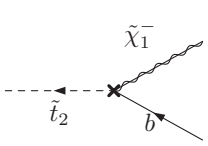
$$\delta[g_{\tilde{t}_1 b \tilde{\chi}_i^-}^{(1)}] = g_{\tilde{t}_1 \tilde{\chi}_i^- b, L}^{(1)} \left[R_{11}^{\tilde{t}} \left(\frac{\delta Z_{b_R} + \delta Z_{\tilde{t}_1}}{2} + \frac{\delta m_b}{m_b} + \delta_{\text{SUSY}} \right) + R_{21}^{\tilde{t}} \frac{\delta Z_{12}^{\tilde{t}}}{2} \right] + g_{\tilde{t}_1 \tilde{\chi}_i^- b, R}^{(1)} \left[R_{12}^{\tilde{t}} \left(\frac{\delta Z_{b_R} + \delta Z_{\tilde{t}_1}}{2} \right) + R_{22}^{\tilde{t}} \frac{\delta Z_{12}^{\tilde{t}}}{2} \right]$$

$$\delta[g_{\tilde{t}_1 b \tilde{\chi}_i^-}^{(2)}] = g_{\tilde{t}_1 \tilde{\chi}_i^- b, L}^{(2)} \left[R_{11}^{\tilde{t}} \left(\frac{\delta Z_{b_L} + \delta Z_{\tilde{t}_1}}{2} + \delta_{\text{SUSY}} \right) + R_{21}^{\tilde{t}} \frac{\delta Z_{12}^{\tilde{t}}}{2} \right] + g_{\tilde{t}_1 \tilde{\chi}_i^- b, R}^{(2)} \left[R_{12}^{\tilde{t}} \left(\frac{\delta Z_{b_L} + \delta Z_{\tilde{t}_1}}{2} + \frac{\delta m_t}{m_t} + \delta_{\text{SUSY}} \right) + R_{22}^{\tilde{t}} \frac{\delta Z_{12}^{\tilde{t}}}{2} \right]$$



$$\delta[g_{\tilde{t}_2 b \tilde{\chi}_i^-}^{(1)}] = g_{\tilde{t}_2 \tilde{\chi}_i^- b, L}^{(1)} \left[R_{21}^{\tilde{t}} \left(\frac{\delta Z_{b_L}^\dagger + \delta Z_{\tilde{t}_2}}{2} + \delta_{\text{SUSY}} \right) + R_{11}^{\tilde{t}} \frac{\delta Z_{12}^{\tilde{t}}}{2} \right] + g_{\tilde{t}_2 \tilde{\chi}_i^- b, R}^{(1)} \left[R_{22}^{\tilde{t}} \left(\frac{\delta Z_{b_L}^\dagger + \delta Z_{\tilde{t}_2}}{2} + \frac{\delta m_t}{m_t} + \delta_{\text{SUSY}} \right) + R_{12}^{\tilde{t}} \frac{\delta Z_{12}^{\tilde{t}}}{2} \right]$$


$$\delta[g_{\tilde{t}_2 b \tilde{\chi}_i^-}^{(2)}] = g_{\tilde{t}_2 \tilde{\chi}_i^- b, L}^{(2)} \left[R_{21}^{\tilde{t}} \left(\frac{\delta Z_{b_R}^\dagger + \delta Z_{\tilde{t}_2}}{2} + \frac{\delta m_b}{m_b} + \delta_{\text{SUSY}} \right) + R_{11}^{\tilde{t}} \frac{\delta Z_{12}^{\tilde{t}}}{2} \right] + g_{\tilde{t}_2 \tilde{\chi}_i^- b, R}^{(2)} \left[R_{22}^{\tilde{t}} \left(\frac{\delta Z_{b_R}^\dagger + \delta Z_{\tilde{t}_2}}{2} + \delta_{\text{SUSY}} \right) + R_{12}^{\tilde{t}} \frac{\delta Z_{12}^{\tilde{t}}}{2} \right]$$




$$\delta[g_{\tilde{t}_2 b \tilde{\chi}_i^-}^{(1)}] = g_{\tilde{t}_2 \tilde{\chi}_i^- b, L}^{(1)} \left[R_{21}^{\tilde{t}} \left(\frac{\delta Z_{b_R} + \delta Z_{\tilde{t}_2} + \frac{\delta m_b}{m_b} + \delta_{\text{SUSY}}}{2} \right) + R_{11}^{\tilde{t}} \frac{\delta Z_{12}^{\tilde{t}}}{2} \right] + g_{\tilde{t}_2 \tilde{\chi}_i^- b, R}^{(1)} \left[R_{22}^{\tilde{t}} \left(\frac{\delta Z_{b_R} + \delta Z_{\tilde{t}_2} + \delta_{\text{SUSY}}}{2} \right) + R_{12}^{\tilde{t}} \frac{\delta Z_{12}^{\tilde{t}}}{2} \right]$$

$$\delta[g_{\tilde{t}_2 b \tilde{\chi}_i^-}^{(2)}] = g_{\tilde{t}_2 \tilde{\chi}_i^- b, L}^{(2)} \left[R_{21}^{\tilde{t}} \left(\frac{\delta Z_{b_L} + \delta Z_{\tilde{t}_2} + \delta_{\text{SUSY}}}{2} \right) + R_{11}^{\tilde{t}} \frac{\delta Z_{12}^{\tilde{t}}}{2} \right] + g_{\tilde{t}_2 \tilde{\chi}_i^- b, R}^{(2)} \left[R_{22}^{\tilde{t}} \left(\frac{\delta Z_{b_L} + \delta Z_{\tilde{t}_2} + \frac{\delta m_t}{m_t} + \delta_{\text{SUSY}}}{2} \right) + R_{12}^{\tilde{t}} \frac{\delta Z_{12}^{\tilde{t}}}{2} \right]$$

Finally, we document the required counterterms to renormalize the UV divergent 2-point functions associated to heavy flavor squarks. Non-diagonal loop-induced transitions $\tilde{q}_1 - \tilde{q}_2$ give rise to additional divergent structures, as compared to light generation squarks:



$$i [(p^2 - m_{\tilde{q}}^2) \delta Z_{\tilde{q}_a} - \delta m_{\tilde{q}_a}^2]$$


$$i \left[p^2 \delta Z_{12}^{\tilde{q}} - \frac{1}{2} (m_{\tilde{q}_1}^2 + m_{\tilde{q}_2}^2) \delta Z_{12}^{\tilde{q}} - \delta Y_{\tilde{q}}^2 \right]$$

-
- [1] D. E. Morrissey, T. Plehn and T. M. P. Tait, Phys. Rept. **515**, 1 (2012).
[2] C. Boehm, P. S. B. Dev, A. Mazumdar and E. Pukartas, JHEP **1306**, 113 (2013); T. Cohen and J. G. Wacker, JHEP **1309**, 061 (2013); A. Fowlie, K. Kowalska, L. Roszkowski, E. M. Sessolo and Y. -L. S. Tsai, Phys. Rev. D **88**, 055012 (2013); S. Henrot-Versille *et al* , Phys. Rev. D **89**, 055017 (2014); P. Bechtle *et al* , arXiv:1310.3045 [hep-ph]; O. Buchmueller *et al* . arXiv:1312.5250 [hep-ph]; J. Ellis, K. A. Olive and J. Zheng, arXiv:1404.5571 [hep-ph].
[3] G. Aad *et al* [ATLAS Collaboration], Phys. Rev. D **87**, 012008 (2013) [arXiv:1208.0949 [hep-ex]]; S. Chatrchyan *et al* [CMS Collaboration], Phys. Rev. Lett. **109**, 171803 (2012) [arXiv:1207.1898 [hep-ex]]; and the most recent (not yet published) updates, cf. e.g. CMS-PAS-SUS-12-028
[4] <https://twiki.cern.ch/twiki/bin/view/AtlasPublic/SupersymmetryPublicResults>
[5] <https://twiki.cern.ch/twiki/bin/view/CMSPublic/PhysicsResultsSUS>
[6] see e.g. B. de Carlos and J. A. Casas, Phys. Lett. B **309**, 320 (1993); M. Dine, R. G. Leigh and A. Kagan, Phys. Rev. D **48**, 4269 (1993); G. W. Anderson and D. J. Castano, Phys. Lett. B **347**, 300 (1995); S. Dimopoulos and G. F. Giudice, Phys. Lett. B **357**, 573 (1995); A. G. Cohen, D. B. Kaplan and A. E. Nelson, Phys. Lett. B **388**, 588 (1996); R. Kitano and Y. Nomura, Phys. Rev. D **73**, 095004 (2006); C. Brust, A. Katz, S. Lawrence and R. Sundrum, JHEP **1203**, 103 (2012); H. M. Lee, V. Sanz and M. Trott, JHEP **1205**, 139 (2012); M. Papucci, J. T. Ruderman and A. Weiler, JHEP **1209**, 035 (2012); J. R. Espinosa, C. Grojean, V. Sanz and M. Trott, JHEP **1212**, 077 (2012); K. Kowalska and E. M. Sessolo, arXiv:1307.5790 [hep-ph]; F. Brümmer, S. Kraml, S. Kulkarni and C. Smith, arXiv:1402.4024 [hep-ph].
[7] H. Baer, V. Barger, P. Huang and X. Tata, JHEP **1205**, 109 (2012); H. Baer and J. List, Phys. Rev. D **88**, 055004 (2013).
[8] O. Buchmueller and J. Marrouche, Int. J. Mod. Phys. A **29**, 1450032 (2014).
[9] F. Brümmer, S. Kraml and S. Kulkarni, JHEP **1208**, 089 (2012).
[10] T. Han, T. Li, S. Su and L. -T. Wang, arXiv:1306.3229 [hep-ph].
[11] J. R. Ellis, K. A. Olive and Y. Santoso, Astropart. Phys. **18**, 395 (2003); C. Boehm, A. Djouadi and M. Drees, Phys. Rev. D **62**, 035012 (2000).
[12] D. E. Morrissey and M. J. Ramsey-Musolf, New J. Phys. **14**, 125003 (2012).
[13] G. Aad *et al* [ATLAS Collaboration], Phys. Rev. Lett. **109**, 211802 (2012); G. Aad *et al* [ATLAS Collaboration], Phys. Rev. Lett. **109**, 211803 (2012); G. Aad *et al* [ATLAS Collaboration], JHEP **1211**, 094 (2012); G. Aad *et al* [ATLAS Collaboration], Eur. Phys. J. C **72**, 2237 (2012); G. Aad *et al* [ATLAS Collaboration], Phys. Lett. B **720**, 13 (2013).
[14] ATLAS-CONF-2013-024, ATLAS-CONF-2013-037; ATLAS-CONF-2013-053; ATLAS-CONF-2013-065
[15] CMS-PAS-SUS-12-023; CMS-PAS-SUS-12-028; CMS-PAS-SUS-13-011
[16] X. -J. Bi, Q. -S. Yan and P. -F. Yin, Phys. Rev. D **85**, 035005 (2012); N. Desai and B. Mukhopadhyaya, JHEP **1205**, 057 (2012); H. K. Dreiner, M. Kramer and J. Tattersall, Europhys. Lett. **99**, 61001 (2012); A. Choudhury and A. Datta, Mod. Phys. Lett. A **27**, 1250188 (2012); R. Mahbubani, M. Papucci, G. Perez, J. T. Ruderman and A. Weiler, Phys. Rev. Lett. **110**, no. 15, 151804 (2013); K. Krizka, A. Kumar and D. E. Morrissey, arXiv:1212.4856 [hep-ph]; C. Han, K. -i. Hikasa, L. Wu, J. M. Yang and Y. Zhang, JHEP **1310**, 216 (2013); J. S. Kim, K. Rolbiecki, K. Sakurai and J. Tattersall, arXiv:1406.0858 [hep-ph]; M. Czakon, A. Mitov, M. Papucci, J. T. Ruderman and A. Weiler, arXiv:1407.1043 [hep-ph].
[17] Z. Han, A. Katz, D. Krohn and M. Reece, JHEP **1208**, 083 (2012); E. L. Berger, Q. -H. Cao, J. -H. Yu and H. Zhang,

- Phys. Rev. Lett. **109**, 152004 (2012); C. Kilic and B. Tweedie, JHEP **1304**, 110 (2013); G. Belanger, R. M. Godbole, L. Hartgring and I. Niessen, JHEP **1305**, 167 (2013); E. L. Berger, Q. -H. Cao, J. -H. Yu and H. Zhang, arXiv:1305.7266 [hep-ph]; X. -Q. Li, Z. -G. Si, K. Wang, L. Wang, L. Zhang and G. Zhu, Phys. Rev. D **89**, 077703 (2014); B. Dutta, W. Flanagan, A. Gurrola, W. Johns, T. Kamon, P. Sheldon, K. Sinha and K. Wang *et al.*, arXiv:1312.1348 [hep-ph].
- [18] M. Drees, M. Hanussek and J. S. Kim, Phys. Rev. D **86**, 035024 (2012); D. S. M. Alves, M. R. Buckley, P. J. Fox, J. D. Lykken and C. -T. Yu, Phys. Rev. D **87**, no. 3, 035016 (2013); B. Dutta, T. Kamon, N. Kolev, K. Sinha and K. Wang, Phys. Rev. D **86**, 075004 (2012); K. Ghosh, K. Huitu, J. Laamanen, L. Leinonen, K. Huitu, J. Laamanen and L. Leinonen, Phys. Rev. Lett. **110**, 141801 (2013); Z. -H. Yu, X. -J. Bi, Q. -S. Yan and P. -F. Yin, Phys. Rev. D **87**, 055007 (2013); M. R. Buckley, T. Plehn and M. J. Ramsey-Musolf, arXiv:1403.2726 [hep-ph].
- [19] S. Kraml and A. R. Raklev, Phys. Rev. D **73**, 075002 (2006); S. Bornhauser, M. Drees, S. Grab and J. S. Kim, Phys. Rev. D **83**, 035008 (2011); B. He, T. Li and Q. Shafi, JHEP **1205**, 148 (2012); C. -Y. Chen, A. Freitas, T. Han and K. S. M. Lee, JHEP **1211**, 124 (2012); C. Han, K. -i. Hikasa, L. Wu, J. M. Yang and Y. Zhang, arXiv:1308.5307 [hep-ph].
- [20] G. L. Kane and J. P. Leveille, Phys. Lett. B **112**, 227 (1982); P. R. Harrison and C. H. Llewellyn Smith, Nucl. Phys. B **213**, 223 (1983) [Erratum-ibid. B **223**, 542 (1983)]; E. Reya and D. P. Roy, Phys. Rev. D **32**, 645 (1985); S. Dawson, E. Eichten and C. Quigg, Phys. Rev. D **31**, 1581 (1985); H. Baer and X. Tata, Phys. Lett. B **160**, 159 (1985).
- [21] W. Beenakker, R. Höpker, M. Spira and P. M. Zerwas, Phys. Rev. Lett. **74**, 2905 (1995); G. Bozzi, B. Fuks and M. Klasen, Phys. Rev. D **72**, 035016 (2005).
- [22] W. Beenakker, R. Höpker, M. Spira and P. M. Zerwas, Z. Phys. C **69**, 163 (1995).
- [23] W. Beenakker, R. Höpker, M. Spira and P. M. Zerwas, Nucl. Phys. B **492** (1997) 51.
- [24] available under www.thphys.uni-heidelberg.de/~plehn
- [25] W. Beenakker, M. Krämer, T. Plehn, M. Spira and P. M. Zerwas, Nucl. Phys. B **515**, 3 (1998).
- [26] S. Bornhauser, M. Drees, H. K. Dreiner and J. S. Kim, Phys. Rev. D **76**, 095020 (2007); W. Hollik, M. Kollar and M. K. Trenkel, JHEP **0802**, 018 (2008); M. Beccaria, G. Macorini, L. Panizzi, F. M. Renard and C. Verzegnassi, Int. J. Mod. Phys. A **23**, 4779 (2008); A. Arhrib, R. Benbrik, K. Cheung and T. -C. Yuan, JHEP **1002**, 048 (2010); W. Hollik, E. Mirabella and M. K. Trenkel, JHEP **0902**, 002 (2009); J. Germer, W. Hollik, E. Mirabella and M. K. Trenkel, JHEP **1008**, 023 (2010); J. Germer, W. Hollik and E. Mirabella, JHEP **1105**, 068 (2011); W. Hollik, J. M. Lindert and D. Pagani, JHEP **1303**, 139 (2013); W. Hollik, J. M. Lindert and D. Pagani, Eur. Phys. J. C **73**, 2410 (2013); J. Germer, W. Hollik, J. M. Lindert and E. Mirabella, arXiv:1404.5572 [hep-ph].
- [27] U. Langenfeld and S. -O. Moch, Phys. Lett. B **675**, 210 (2009); U. Langenfeld, S. -O. Moch and T. Pfoh, JHEP **1211**, 070 (2012).
- [28] W. Beenakker, S. Brensing, M. Krämer, A. Kulesza, E. Laenen and I. Niessen, JHEP **0912**, 041 (2009); J. Debove, B. Fuks and M. Klasen, Nucl. Phys. B **849**, 64 (2011); A. Kulesza and L. Motyka, Phys. Rev. Lett. **102**, 111802 (2009); A. Kulesza and L. Motyka, Phys. Rev. D **80**, 095004 (2009); M. Beneke, P. Falgari and C. Schwinn, Nucl. Phys. B **842**, 414 (2011); P. Falgari, C. Schwinn and C. Wever, JHEP **1206**, 052 (2012); M. R. Kauth, J. H. Kühn, P. Marquard and M. Steinhauser, Nucl. Phys. B **857**, 28 (2012).
- [29] R. Gavin, C. Hangst, M. Krämer, M. Mühlleitner, M. Pellen, E. Popenza and M. Spira, arXiv:1305.4061 [hep-ph].
- [30] T. Binoth, D. Gonçalves-Netto, D. López-Val, K. Mawatari, T. Plehn and I. Wigmore, Phys. Rev. D **84**, 075005 (2011).
- [31] D. Gonçalves-Netto, D. López-Val, K. Mawatari, T. Plehn and I. Wigmore, Phys. Rev. D **87**, 014002 (2013).
- [32] D. Gonçalves-Netto, D. López-Val, K. Mawatari, T. Plehn and I. Wigmore, Phys. Rev. D **85**, 114024 (2012); D. Gonçalves-Netto, D. López-Val, K. Mawatari, I. Wigmore and T. Plehn, Phys. Rev. D **87**, 094023 (2013).
- [33] J. Alwall *et al.*, JHEP **0709**, 028 (2007).
- [34] J. Alwall, M. Herquet, F. Maltoni, O. Mattelaer and T. Stelzer, JHEP **1106**, 128 (2011).
- [35] P. Nogueira, J. Comp. Phys. **105**, 279 (1993).
- [36] T. Binoth, J. P. Guillet, G. Heinrich, E. Pilon and C. Schubert, JHEP **0510** (2005) 015; G. Cullen, N. Greiner, A. Guffanti, J. P. Guillet, G. Heinrich, S. Karg, N. Kauer, T. Kleinschmidt *et al.*, Nucl. Phys. Proc. Suppl. **205-206** (2010) 67-73.
- [37] T. Binoth, J. P. Guillet, G. Heinrich, E. Pilon and T. Reiter, Comput. Phys. Commun. **180**, 2317 (2009); G. Cullen, J. P. Guillet, G. Heinrich, T. Kleinschmidt, E. Pilon, T. Reiter and M. Rodgers, Comput. Phys. Commun. **182**, 2276 (2011).
- [38] S. Catani and M. H. Seymour, Nucl. Phys. B **485**, 291 (1997) [Erratum-ibid. B **510**, 503 (1998)]; S. Catani, S. Dittmaier, M. H. Seymour and Z. Trocsanyi, Nucl. Phys. B **627**, 189 (2002).
- [39] for some more details see e.g. T. Plehn, C. Weydert, PoS **CHARGED2010**, 026 (2010).
- [40] R. Frederix, T. Gehrmann and N. Greiner, JHEP **0809**, 122 (2008); and JHEP **1006**, 086 (2010).
- [41] S. Frixione, Z. Kunszt and A. Signer, Nucl. Phys. B **467**, 399 (1996); Z. Nagy and Z. Trocsanyi, Phys. Rev. D **59**, 014020 (1999) [Erratum-ibid. D **62**, 099902 (2000)].
- [42] S. P. Martin and M. T. Vaughn, Phys. Lett. B **318**, 331 (1993); A. Signer, D. Stöckinger, Phys. Lett. **B626**, 127-138 (2005); and Nucl. Phys. **B808**, 88-120 (2009).
- [43] J. Pumplin, D. R. Stump, J. Huston, H. L. Lai, P. Nadolsky and W. K. Tung, JHEP **0207**, 012 (2002).
- [44] R. D. Ball, V. Bertone, F. Cerutti, L. Del Debbio, S. Forte, A. Guffanti, J. I. Latorre and J. Rojo *et al.*, Nucl. Phys. B **849**, 296 (2011).
- [45] C. F. Berger, J. S. Gainer, J. L. Hewett and T. G. Rizzo, JHEP **0902**, 023 (2009).
- [46] M. W. Cahill-Rowley, J. L. Hewett, A. Ismail, M. E. Peskin and T. G. Rizzo, arXiv:1305.2419 [hep-ph].
- [47] S. S. AbdusSalam, B. C. Allanach, H. K. Dreiner, J. Ellis, U. Ellwanger, J. Gunion, S. Heinemeyer and M. Krämer *et al.*, Eur. Phys. J. C **71**, 1835 (2011).
- [48] B. C. Allanach, Comput. Phys. Commun. **143**, 305 (2002).
- [49] T. Sjöstrand, S. Mrenna and P. Z. Skands, JHEP **0605**, 026 (2006).
- [50] M. L. Mangano, M. Moretti, and R. Pittau, Nucl. Phys. B **632**, 343 (2002).

- [51] J. Alwall, S. de Visscher, F. Maltoni, JHEP **0902**, 017 (2009).
- [52] T. Plehn, D. Rainwater, P. Z. Skands, Phys. Lett. **B645**, 217-221 (2007); T. Plehn and T. M. P. Tait, J. Phys. G **36**, 075001 (2009).
- [53] C. Englert, T. Plehn, P. Schichtel and S. Schumann, Phys. Rev. D **83**, 095009 (2011).
- [54] T. Plehn, Phys. Rev. D **67**, 014018 (2003); E. Boos and T. Plehn, Phys. Rev. D **69**, 094005 (2004).
- [55] J. C. Collins and W. -K. Tung, Nucl. Phys. B **278**, 934 (1986); R. M. Barnett, H. E. Haber and D. E. Soper, Nucl. Phys. B **306**, 697 (1988). F. I. Olness and W. -K. Tung, Nucl. Phys. B **308**, 813 (1988). M. A. G. Aivazis, J. C. Collins, F. I. Olness and W. -K. Tung, Phys. Rev. D **50**, 3102 (1994); J. C. Collins, Phys. Rev. D **58**, 094002 (1998); M. Krämer, F. I. Olness and D. E. Soper, Phys. Rev. D **62**, 096007 (2000).
- [56] for a recent overview see e.g. F. Maltoni, G. Ridolfi and M. Ubiali, JHEP **1207**, 022 (2012) [Erratum-ibid. **1304**, 095 (2013)].
- [57] F. Maltoni, Z. Sullivan and S. Willenbrock, Phys. Rev. D **67**, 093005 (2003); S. Dawson, C. B. Jackson, L. Reina and D. Wackerroth, Mod. Phys. Lett. A **21**, 89 (2006); R. V. Harlander and W. B. Kilgore, Phys. Rev. Lett. **88**, 201801 (2002).
- [58] W. Beenakker, R. Höpker and P. M. Zerwas, Phys. Lett. B **378**, 159 (1996); S. Kraml, H. Eberl, A. Bartl, W. Majerotto and W. Porod, Phys. Lett. B **386**, 175 (1996); A. Djouadi, W. Hollik and C. Jünger, Phys. Rev. D **55**, 6975 (1997); W. Beenakker, R. Höpker, T. Plehn and P. M. Zerwas, Z. Phys. C **75**, 349 (1997); J. Guasch, J. Solà and W. Hollik, Phys. Lett. B **437**, 88 (1998); A. Bartl, H. Eberl, K. Hidaka, S. Kraml, W. Majerotto, W. Porod and Y. Yamada, Phys. Rev. D **59**, 115007 (1999); M. Mühlleitner, A. Djouadi and Y. Mambrini, Comput. Phys. Commun. **168**, 46 (2005); L. G. Jin and C. S. Li, Phys. Rev. D **65**, 035007 (2002); J. Guasch, W. Hollik and J. Solà, Phys. Lett. B **510**, 211 (2001); J. Guasch, W. Hollik and J. Solà, JHEP **0210**, 040 (2002); A. Arhrib and R. Benbrik, Phys. Rev. D **71**, 095001 (2005).
- [59] W. Hollik and H. Rzehak, Eur. Phys. J. C **32**, 127 (2003).
- [60] M. A. Diaz, hep-ph/9705471; T. Plehn and W. Beenakker, In *Barcelona 1997, Quantum effects in the minimal supersymmetric standard model* 244-249.
- [61] Q. Li, L. G. Jin and C. S. Li, Phys. Rev. D **66**, 115008 (2002); C. Weber, K. Kovarik, H. Eberl and W. Majerotto, Nucl. Phys. B **776**, 138 (2007).
- [62] A. Djouadi, P. Gambino, S. Heinemeyer, W. Hollik, C. Jünger and G. Weiglein, Phys. Rev. D **57**, 4179 (1998); S. Heinemeyer, W. Hollik, H. Rzehak and G. Weiglein, Eur. Phys. J. C **39**, 465 (2005); N. Baro and F. Boudjema, Phys. Rev. D **80**, 076010 (2009).
- [63] S. Heinemeyer, H. Rzehak and C. Schappacher, Phys. Rev. D **82**, 075010 (2010).
- [64] S. Heinemeyer, W. Hollik, H. Rzehak and G. Weiglein, Phys. Lett. B **652**, 300 (2007); T. Fritzsche, S. Heinemeyer, H. Rzehak and C. Schappacher, Phys. Rev. D **86**, 035014 (2012).
- [65] W. Hollik, E. Kraus, M. Roth, C. Rupp, K. Sibold and D. Stöckinger, Nucl. Phys. B **639**, 3 (2002).
- [66] S. Berge, W. Hollik, W. M. Mosle and D. Wackerroth, Phys. Rev. D **76**, 034016 (2007).
- [67] J. C. Collins, F. Wilczek and A. Zee, Phys. Rev. D **18**, 242 (1978).
- [68] A. van Hameren, Comput. Phys. Commun. **182**, 2427 (2011).
- [69] T. Fritzsche and W. Hollik, Eur. Phys. J. C **24**, 619 (2002).